Paper A

Detecting Eccentricity and Demagnetization Fault of Permanent Magnet Synchronous Generators in Transient State

Sveinung Attestog, Huynh Van Khang, Kjell G. Robbersmyr

This paper has been published as:

S. Attestog, H. V. Khang and K. G. Robbersmyr, "Detecting Eccentricity and Demagnetization Fault of Permanent Magnet Synchronous Generators in Transient State," 2019 22nd International Conference on Electrical Machines and Systems (ICEMS), Harbin, China, 2019, pp. 1-5, doi: 10.1109/ICEMS.2019.8921753.

A.1 Abstract

Eccentricity and demagnetization fault of a four-pole 1.5 kW surface mounted permanent-magnet synchronous-generator (PMSG) were modelled by using time-discretised finite element analysis (FEA). Both fault types are caused by magnetic asymmetry in the generator. The faulty behaviour of a PMSG under transient operating condition is studied with FEA. Two search coils were wound around stator teeth on opposite sides of the rotor. The induced voltage from these coils will be equal in healthy case. A fault is detected when the induced voltages are non-identical. The simulation results revealed that the envelope of the induced search coil voltage had sinusoids during dynamic eccentricity and demagnetization. Finally, a novel fault scheme is proposed to detect the mentioned faults during transient state.

A.2 Introduction

Wind turbine systems are usually based on doubled-fed induction generators or permanent magnet synchronous generators (PMSG). PMSG is gaining in popularity thanks to its simple structure, efficient energy conversion and low noise [1]. Offshore wind has been of interest for a long time. One of the main barriers is the cost of maintenance. Faults in permanent magnet synchronous machines are often caused by contamination, humidity, mechanical tensions, overloading, high temperature, vibrations, and the partial discharge of high-frequency switching from frequency converters [2]. The detection and identification of faults in PMSGs in earlier stages is critical for safe, profitable and reliable operation of offshore wind turbines.

The most common fault types in PMSGs are inter-turn short circuit, irreversible demagnetisation, and rotor eccentricity. The most popular fault detection technique in commercial use is machine current signal analysis (MCSA) where Fast Fourier Transform is used for processing the machine current signal. The faults is identified according to certain harmonic patterns. The technique is limited to stationary operating condition. Motors in electric vehicles and generators in wind turbine often operate with varying speed and load. Short-Time Fourier−, Wavelet-, and Hilbert Huang Transform are then used for analysis in transient operating conditions. Alternatively, the data generated is fed into an artificial neural network, being trained to classify the different fault patterns [3].

One of the best indicators for detecting mechanical faults like static and dynamic eccentricity is vibration signatures. The fault is detected by analysing the measured vibrations using signal processing techniques to identify the signature for a certain fault [4]. Another methods for detecting local demagnetisation and eccentricity is using analytical model based on an inverse problem [5]. A well design analytical or lumped magnetic circuit model can detect faults based on the measured terminal voltage, current and torque. An online detection method was presented in [6], which could detect local demagnetisation and dynamic eccentricity based on measurement from the Hall sensor [6].

Fault detection schemes involving search coils are intensively developed. The authors in [7] presented a fault detection scheme to detect asymmetry in the magnetic circuit of

a permanent magnet synchronous motor (PMSM). Twelve search coils are placed evenly spaced in the stator wound around their own stator tooth. The fault detection scheme used linear time-invariant filter for tracking of the fundamental component of the induced search coil voltage. This is then used to produce polar plots. The radius represents the amplitude of the induced voltage in the search coil and the angle represents the locations of the search coils. The shape of the polar plot indicated what type of faults was occurring in the electrical machine [7]. The amplitude of the induced search coil voltage is dependent on the speed of the electrical machine. This does not affect the overall shape of the polar plots, but false alarms may occur due to transient operating conditions. Unless all induced search coil voltages increase at the same rate simultaneously, keeping the shape of the polar plot.

This paper will investigate the possibility of a fault classifier for differentiating demagnetisation, static eccentricity and dynamic eccentricity. It is inspired by the fault detection scheme in [7]. The main contribution is to propose a detection scheme to detect the mentioned faults by using a fewer search coils.

A.3 Finite Element Analysis PMSG

A 1.5 kW 4-pole surface-mounted PMSG with sinusoidally distributed double layer windings was simulated. The geometry of the model is shown in Figure A.1 and is based on the motor design in [8]. The windings in each slot are divided into two coil-domains, where each of them represents a bundle of 40 turns. The model is first solved in a stationary solver where the rotor is standing still (Without applied torque or terminal voltage). This result is used as the initial conditions for the time-stepping finite element analysis (FEA). The governing equations of the electromagnetic model are below

$$\nabla \times \boldsymbol{H} = \boldsymbol{J}, \tag{A.1}$$

$$\boldsymbol{B} = \nabla \times \boldsymbol{A}, \tag{A.2}$$

$$\boldsymbol{E} = -\frac{\partial \boldsymbol{A}}{\partial t}, \tag{A.3}$$

and

$$\nabla \cdot \boldsymbol{B} = 0. \tag{A.4}$$

where $\boldsymbol{H}$ is the magnetic flux intensity, $\boldsymbol{J}$ is the current density, $\boldsymbol{B}$ is the magnetic flux density, $\boldsymbol{A}$ is the magnetic vector potential and $\boldsymbol{E}$ is the electric field intensity. The magnets are described with the linear model[9]

$$\boldsymbol{B} = \mu_r \mu_0 \boldsymbol{H} + \boldsymbol{B_r}. \tag{A.5}$$

where μ_0 is the permeability in vacuum and the relative permeability μ_r is set to 1. The remanence magnetic flux $\boldsymbol{B_r}$ is set to 0.5 T and is reduced to 0.4 T for modelling demagnetised magnet.

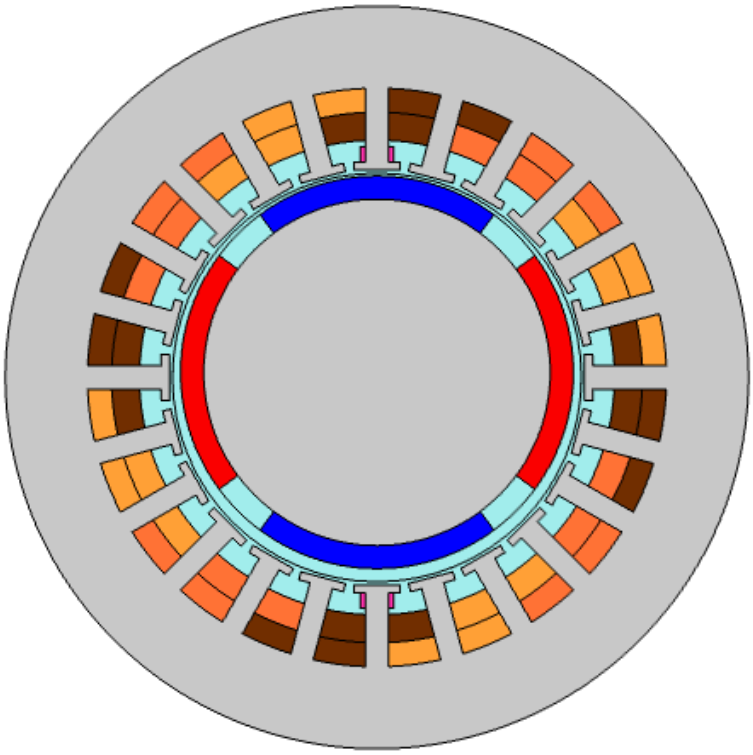

Figure A.1: PMSG Model geometry

A.4 Proposed fault detection and classification scheme

A.4.1 Fault indicator

The proposed method for fault detection is to compare the signal of two strategically placed search coils. The first search coil can be wound around any stator tooth. The second coil needs to be wound around the stator tooth located on the opposite side of the rotor. The voltage signal from these two search coils will theoretically be identical due to the geometry. Due to this criterion, this method works best on electrical machines with even number of stator teeth. The proposed fault indicator is:

$$F_{\text{Det}} = (V_{C1} - V_{C2})^2. \tag{A.6}$$

where V_{C1} and V_{C2} are the induced voltage in search coil 1 and 2, respectively. If F_{Det} is 0, then no fault is detected, and if it is not equal to 0 a magnetic asymmetry is detected. This is the case when the measurement has no noise. Measurements from a real sensor will of course have noise. In this case, a threshold δ needs to be selected based on an estimated variance in the signal. A fault is detected when F_{Det} is greater than δ.

A.4.2 Fault Classifier

Originally the suggested classifier for this paper was:

$$F_{\text{Class}} = \left((a \sin\left(\omega(t)t + \phi\right) + k_1\right)^2 + \left(b \cos\left(\omega(t)t + \phi\right) + k_2\right)^2\right)^{0.5}. \tag{A.7}$$

where a, b, k_1 and k_2 are shape fitting parameters of the envelope. The time varying angular frequency $\omega(t)$ can be written as $f(t)$, where $f(t)$ is time varying frequency. The fundamental frequency of the envelope is approximately a half of the fundamental frequency to the original induced search coil voltage. This is shown later in the results. Neither $\omega(t)$ or phase angle ϕ are used for classification of the faults in the generator, but are important for fitting the curve. Equation (A.7) is inspired by the polar plots in [7]. If no fault was present in the machine, the shape of the polar plots was a perfect circle. In the case of static eccentricity, the circle was move off centre. Assuming that the speed was constant, the envelope of the induced search coil voltage will be constant over time in both cases. The polar plots in the cases of dynamic eccentricity and demagnetisation had a rotating movement over time. This will also be reflected in the envelop pattern in the induced search coil voltage.

All the parameters used to classify faults in (A.7) have a physical meaning in terms of the dynamic eccentricity and demagnetisation. Dynamic eccentricity is detected if $k_1 \neq 0$ or $k_2 \neq 0$ and demagnetisation is detected if a $\neq$ b. The equation is difficult to work with, thus it is replaced with:

$$F_{\text{Class}} = A \cos\left(2\omega(t)t + \phi\right) + B \cos\left(\omega(t)t + \phi\right) + h(t). \tag{A.8}$$

Derivation of the expression inside the square root in (A.7) will result in an equation with similar shape as (A.8). Both equation can fit the envelop of the induced search coil voltage equally well. Some information is lost in the simplification, but (A.8) is still sufficient for fitting the envelope curve for classification of faults. The parameters A and B is still loosely related to the original classification parameter a, b, k_1 and k_2. The classification algorithm based on (A.8) is shown in Figure A.2. The classification of fault types depends on whether amplitude A or B is larger than 0. It is assumed that $h(t)$ is proportional to the speed of the rotor. In this study case, it has the shape of a step response of the first order system. Both steady state value and time constant of $h(t)$ can be estimated by minimizing the square error between the envelope curve and $h(t)$. A and B is then estimated by minimizing the square error between data and (A.8) with respect to A, B, ϕ and steady state value of $\omega(t)$. Function $\omega(t)$ is assumed to be the step response of a first order system with same time constant as $h(t)$. Alternative methods for detecting the presence of the sinusoids in the envelope could have been short time Fourier transform or the best linear unbiased estimator (BLUE).

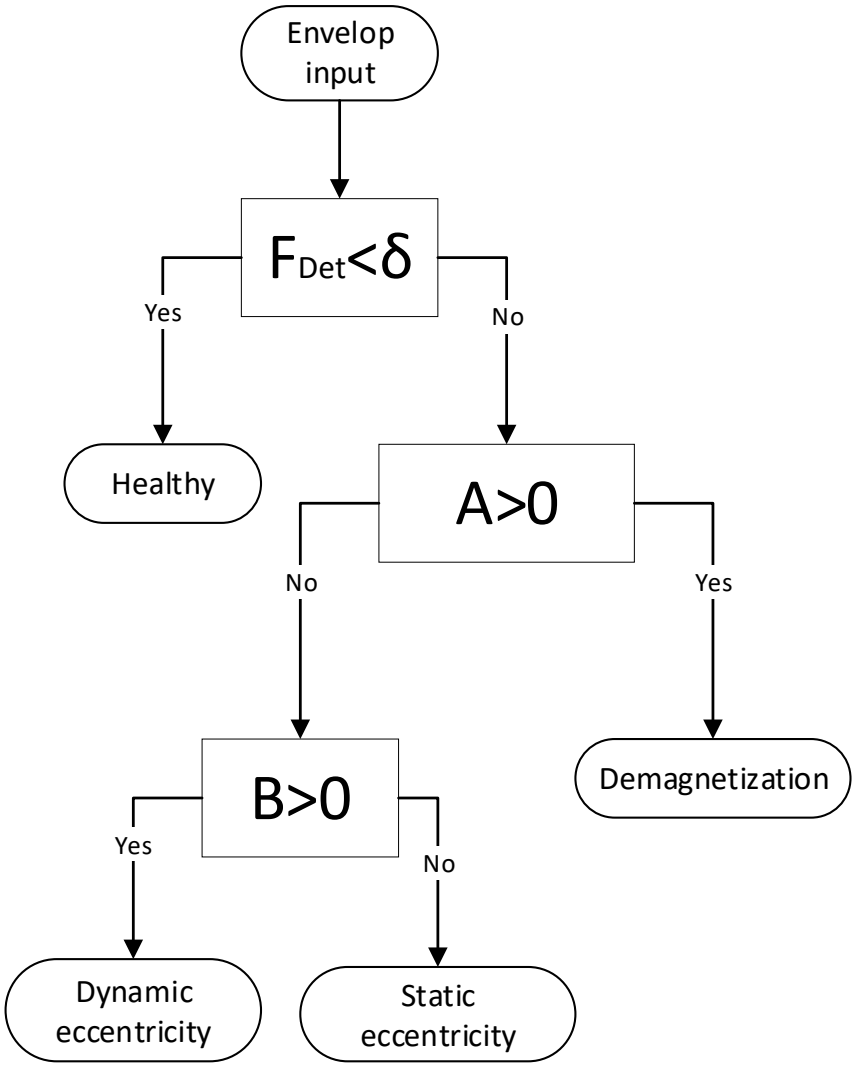

Figure A.2: Suggested fault classification scheme

A.4.3 Simulation

The fault classifier proposed in this paper was tested against simulation training data. The finite element model of the PMSG was run in four different scenarios:

- Healthy: Rotor and stator are concentric and no demagnetised magnets.
- Demagnetisation: Rotor and stator are concentric, but B_r for one South pole is reduced to 0.4 T.
- Static eccentricity: No demagnetised magnet. Rotor and stator are eccentric, but rotating domain shares centre with rotor. The severity is 23.0 %
- Dynamic eccentricity: No demagnetised magnets. Rotor and stator are eccentric, but rotating domain shares centre with stator. The severity is 23.0 %.

In all four scenarios, the rotor had a 10 Nm applied prime mover torque, and the terminals were star-connected to a resistive load of 50 Ω on each phase. Figure A.3 illustrates the difference between the static and dynamic eccentricity. S, R and RD indicates the centres for the stator-, rotor- and rotating domain, respectively. The sketch is exaggerated for better illustrating the difference between the two types of eccentricities.

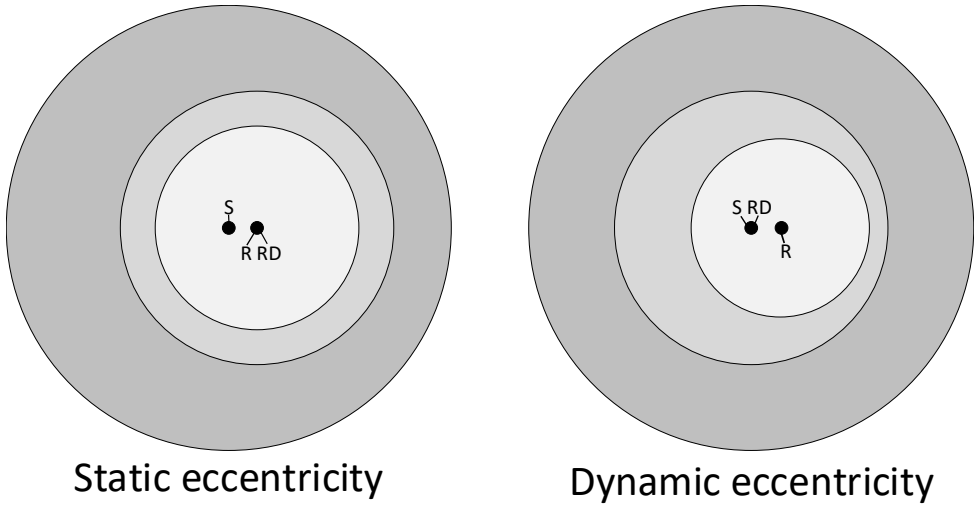

Figure A.3: Simple sketch of modelled eccentricities

A.5 Results and Discussion

Figs. A.4, A.5 and A.6 show the voltage difference between two search coils and the phase current of the PMSG in the beginning of the simulation. The search coils are located on top and bottom of the stator wound around their own stator tooth. The plots on the left side of these figures reveal that the magnetic asymmetry can effectively be detected by the voltage difference between two strategically placed search coils. The phase current is not that simple. A sinusoid is generated in all three faulty cases, which looks similar to the healthy case.

Figs. A.7a and A.7b show the plots of the absolute value of the search coils voltage in healthy case and with static eccentricity fault, respectively. The measurement period plotted in the figures was picked early in the simulation. The induced voltage has some transient behaviour and both the amplitude and frequency are increasing. Both the envelopes of the healthy case and static eccentricity case is increasing steadily. No sinusoidal components is present in the envelope signal. On the other hand, the sinusoidal components are clearly present in the case of demagnetisation and dynamic eccentricity. This is observed in Figs. A.8a and A.8b. The amplitude and frequency of the envelope seem to increase over time when the amplitude and frequency of the original voltage signal also increase. The main frequency component of the envelope curve seems to be a half of fundamental frequency of the original signal. In the case of dynamic eccentricity, the peaks of envelope curve appears at every fourth peaks of the absolute value of the induced search coil voltage. Note that two peaks indicate one period for the absolute value of the

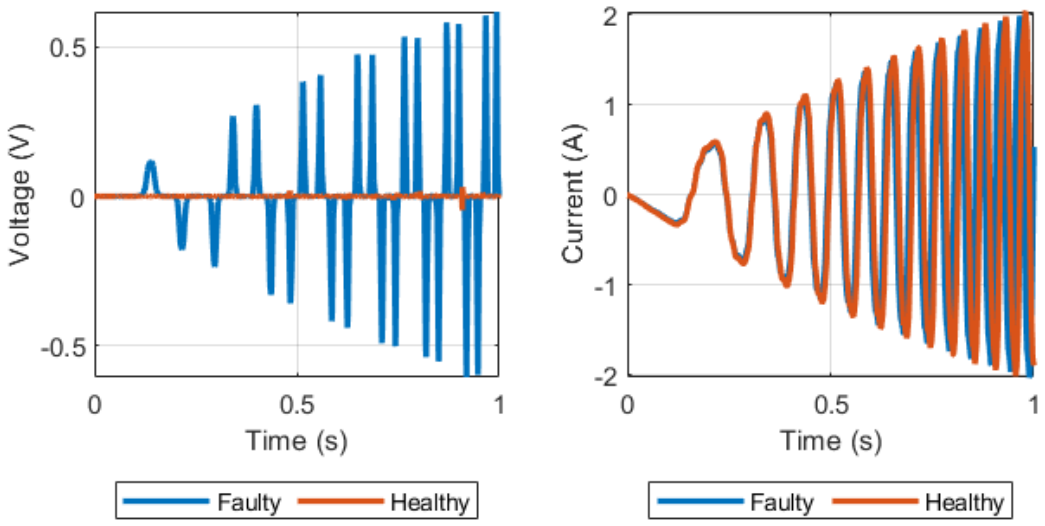

Figure A.4: Demagnetisation - Voltage difference between two strategically placed search coils (left) and phase current (right)

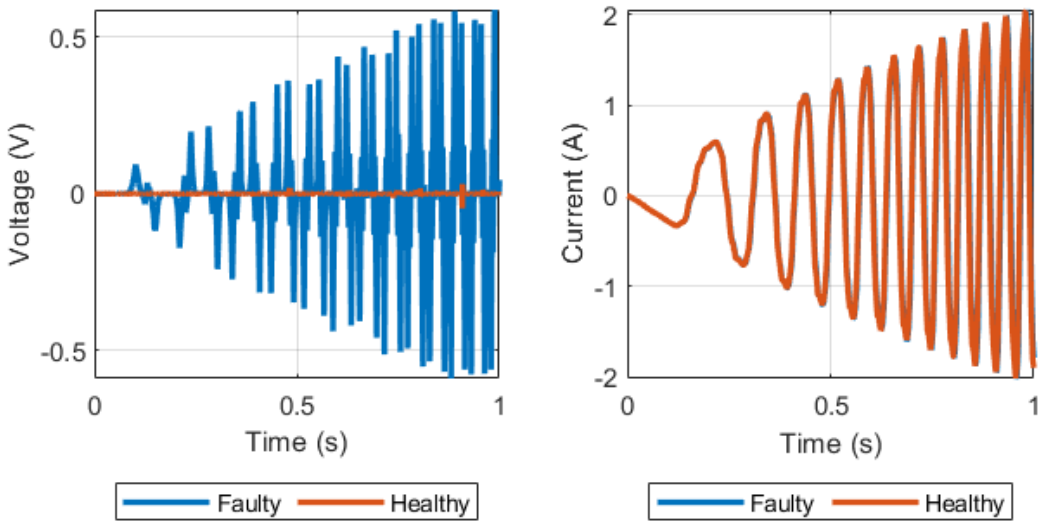

Figure A.5: Static eccentricity - Voltage difference between two strategically placed search coils (left) and phase current (right)

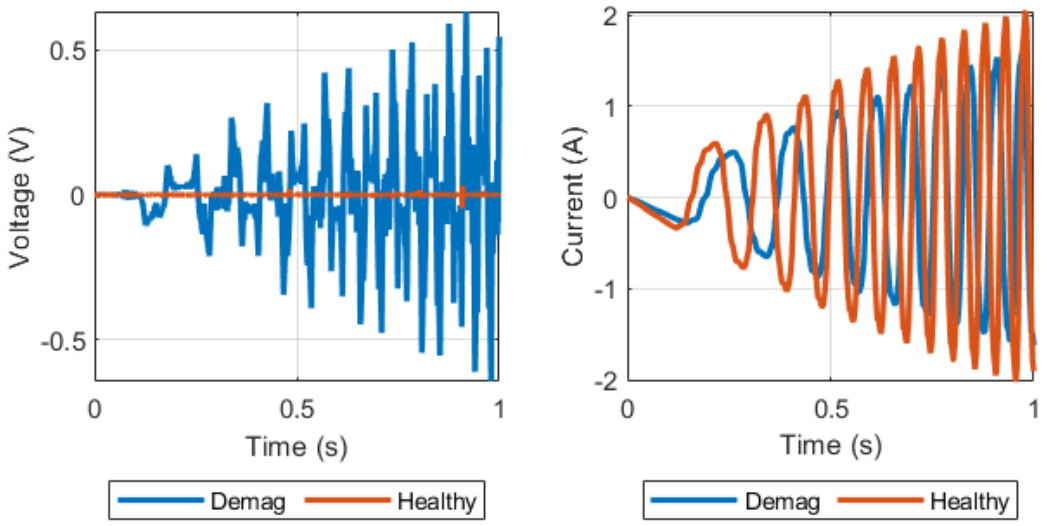

Figure A.6: Dynamic eccentricity - Voltage difference between two strategically placed search coils (left) and phase current (right)

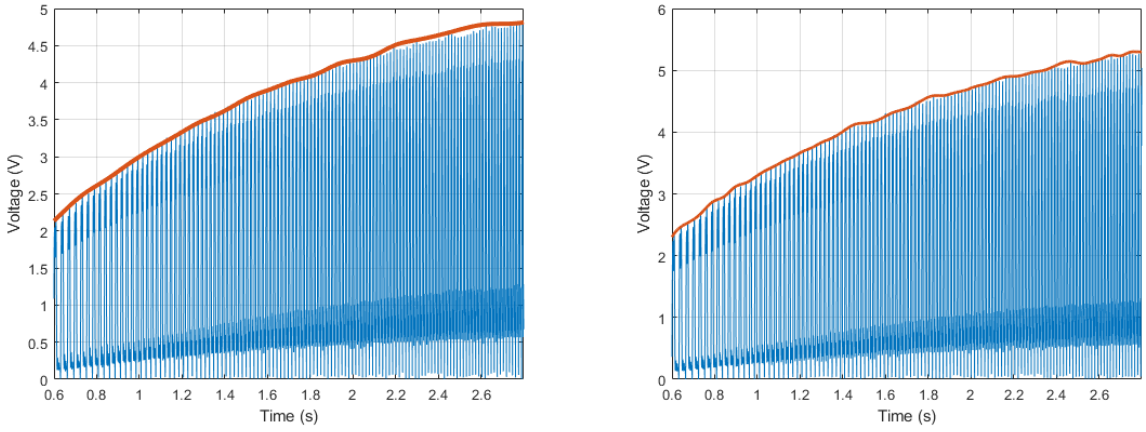

(a) (b)

Figure A.7: Envelope of absolute value of search coil voltage with (a) no faults and (b) static eccentricity fault

search coil voltage, thus the fundamental frequency of the envelope curve is half of the fundamental frequency of the induced search coil voltage.

The envelope curve in Figs. A.7a to A.8a is computed by the "envelope" function in MATLAB. The technique, being proved to be most effective, was the peak value technique. It tracks the maximum values (peaks) of a certain number of last data points. This number was set as 80, but this can vary depending on the data. The number can not be too large or too small. Neither case will not track the envelope and capture its characteristics.

Table A.1 shows the values of the amplitudes A and B from (A.8) in the voltage signal generated from the simulation. The parameters are estimated by minimising the

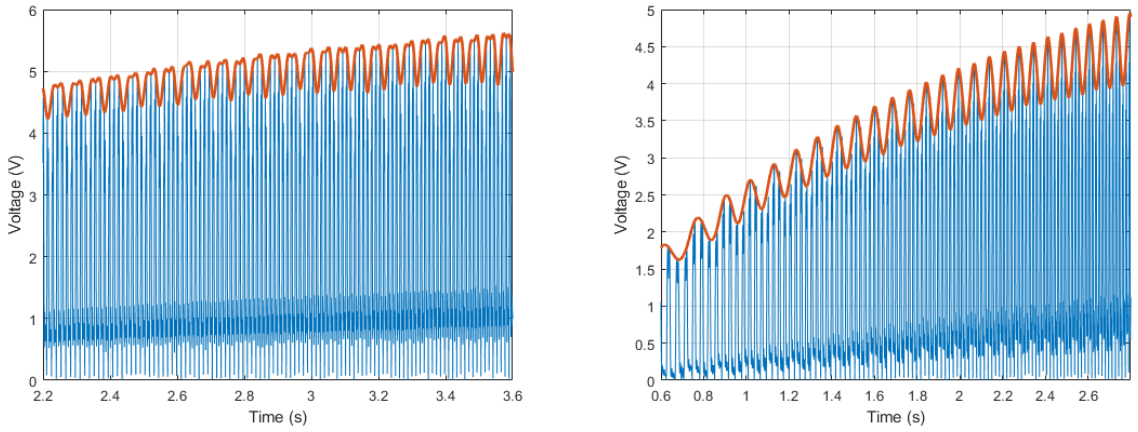

(a) (b)

Figure A.8: Envelope of absolute value of search coil voltage with (a) demagnetisation fault and (b) dynamic eccentricity

Table A.1: Estimated amplitude of sinusoids in the envelope curve

Type of fault	A	B
No-fault	0.0	0.0
Static Eccentricity	0.0	0.0
Dynamic Eccentricity	0.02	0.33
Demagnetisation	0.11	0.25

two objective functions. In the case of demagnetisation, the dataset shown in Figure A.4 includes 18001 data points in the period between 2.20 s and 2.66 s. This set was used to estimate the parameters in function $h(t)$. A smaller subset of 4596 data point was used to estimate A and B. The dataset of the envelope curve from the remaining study cases are shown in Figs. A.7a, A.7b and A.8b including 14001 data points each. A smaller subset of 3096 data points in period between 1.40 s and 1.71 seconds were used to estimate A and B. Both A and B were equal to 0 in healthy case and static eccentricity case. B was present during dynamic eccentricity and both A and B had a larger value than 0 when the PMSG was demagnetised.

The critical point for the fault classifier is the computing of the envelope. If the signal is too noisy, then the fault of the PMSG can not be classified. The noise can be reduced by filtering the signal, low pass filter, moving average filter or Savitzky-Golay filter. The current method for computing the envelope is by taking the maximum from the last data points. The envelope is captured at some parts of the dataset. Figure A.7a to Figure A.8b show some examples where the envelope was captured. The issue with the current simple method is that it will not capture the characteristics of the envelope when the fundamental frequency of the induced voltage is too small or too large. This could be solved with an algorithm where the number of data-points used for computing the envelope varies over time depending on the current fundamental frequency of the induced voltage. This will depend on the speed of the rotor.

A.6 Conclusion

In this paper, a new fault detection scheme was proposed using only 2 search coils. The difference in voltage signals from two strategically placed search coils, being in opposite sides of the rotor, can in theory detect magnetic asymmetry in the generator. The criterion for placing the search coils limits this method to permanent magnet machines with even number of stator teeth. The fault classification scheme was tested on simulations from a finite element model of a PMSG, but will probably also work for a PMSM. Datasets of the induced search coil voltage during transient state operation of the PMSG were extracted, and sinusoidal components in the envelope was identified by minimising two objective functions. Both study cases, with static eccentricity and no fault, had no sinusoidal components. Either one or two sinusoidal component were present during dynamic eccentric case or demagnetisation case, respectively.

Future work will involve experimental verification of the fault classifier and a change in the algorithm that makes it more automatic. This will make the classifier able to classify the fault faster. The alternatives may be to use BLUE or an artificial neural network which is trained to recognise envelope patterns discussed in this paper.

References

[1] B. Yang, T. Yu, H. Shu, *et al.*, "Passivity-based sliding-mode control design for optimal power extraction of a PMSG based variable speed wind turbine," *Renewable Energy*, vol. 119, pp. 577–589, Apr. 2018.

[2] N. Nishiyama, H. Uemura, and Y. Honda, "Highly Demagnetization Performance IPMSM Under Hot Environments," *IEEE Transactions on Industry Applications*, vol. 55, no. 1, pp. 265–272, Feb. 2019.

[3] Z. Ullah and J. Hur, "A Comprehensive Review of Winding Short Circuit Fault and Irreversible Demagnetization Fault Detection in PM Type Machines," *Energies*, vol. 11, no. 12, Nov. 2018.

[4] F. Cira, "Detection of eccentricity fault based on vibration in the PMSM," *Results in physics*, vol. 10, pp. 760–765, Sep. 2018.

[5] J. De Bisschop, A. A. E. Abdallh, P. Sergeant, and L. Dupré, "Analysis and selection of harmonics sensitive to demagnetisation faults intended for condition monitoring of double rotor axial flux permanent magnet synchronous machines," *IET Electric Power Applications*, vol. 12, no. 4, pp. 486–493, Apr. 2018.

[6] Y. Park, D. Fernandez, S. B. Lee, *et al.*, "Online Detection of Rotor Eccentricity and Demagnetization Faults in PMSMs Based on Hall-Effect Field Sensor Measurements," *IEEE Transactions on Industry Applications*, vol. 55, no. 3, pp. 2499–2509, May 2019.

[7] Y. Da, X. Shi, and M. Krishnamurthy, "A New Approach to Fault Diagnostics for Permanent Magnet Synchronous Machines Using Electromagnetic Signature Analysis," *IEEE Transactions on Power Electronics*, vol. 28, no. 8, pp. 4104–4112, Aug. 2013.

[8] B. N. Cassimere, S. D. Sudhoff, and D. H. Sudhoff, "Analytical Design Model for Surface-Mounted Permanent-Magnet Synchronous Machines," *IEEE Transactions on Energy Conversion*, vol. 24, no. 2, pp. 347–357, Jun. 2009.

[9] S. Ruoho, E. Dlala, and A. Arkkio, "Comparison of Demagnetization Models for Finite-Element Analysis of Permanent-Magnet Synchronous Machines," *IEEE Transactions on Magnetics*, vol. 43, no. 11, pp. 3964–3968, Nov. 2007.